



Influence of Hydrogen Pre-treatment at Different Temperatures on Copper Oxide Supported on Carbonised Oil Palm Empty Fruit Bunch (CuO/EFBC) for Low-Temperature Nitric Oxide Removal

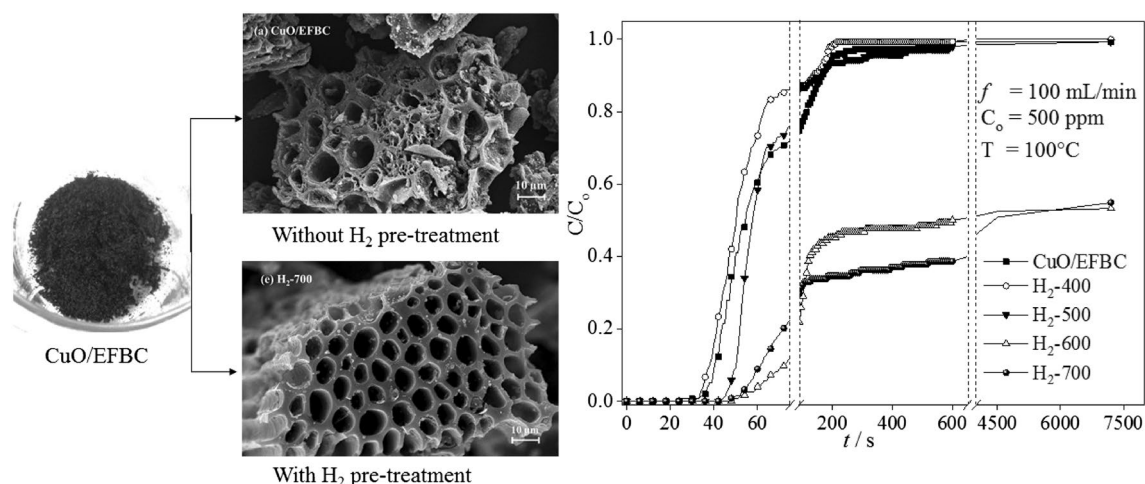
N. Ahmad¹ · F. M. Zahari¹ · N. Ibrahim¹

Received: 6 October 2019 / Accepted: 7 April 2020 / Published online: 13 April 2020
© Springer Nature B.V. 2020

Abstract

Low-temperature nitric oxide (NO) removal by oil palm empty fruit bunch (EFBC) modified with phosphoric acid dehydration, followed by copper oxide (CuO) impregnation is a function of both surface chemical and physical properties of CuO/EFBC resulting from hydrogen (H₂) pre-treatment at different temperatures. Subjecting CuO/EFBC sample to H₂ pre-treatment at 400 °C initially reduces the NO adsorption capacity (q) (at $C/C_0 = 0.95$) from 1.65 to 1.57 mg/g although the BET specific surface area (S_{BET}) increases from 4.81 to 160 m²/g, due to surface predomination by acidic oxygenated groups (e.g. carboxyl, lactone and phenolic groups). At 500 °C, q increases to 5.67 mg/g as some of the acidic surface groups are decomposed and the S_{BET} improves to 466 m²/g. Further increase in the temperature to 600 and 700 °C respectively enhances the S_{BET} to 448 and 516 m²/g, and decomposes most of the acidic groups, leaving unsaturated C to react with H and form stable basic sites e.g. aldehyde, alkane, alkyl and aromatic groups more favourable for NO adsorption, thus giving rise to q (at $C/C_0 = 0.5$) to 41.01 and 62.74 mg/g, with stable performance for more than 2 h of experiment. In addition, higher pore volume, smaller pore size and smaller crystallite size of CuO, Cu₂O and Cu₃P sites are observed in samples pre-treated at high temperatures (600 and 700 °C), leading to a condition more auspicious for dissociative NO adsorption.

Graphic Abstract



Keywords Nitric oxide removal · Hydrogen pre-treatment · Thermal pre-treatment · Copper oxide · Oil palm empty fruit bunch

✉ N. Ibrahim
naimah@unimap.edu.my

Extended author information available on the last page of the article

Statement of Novelty

The use of non-noble metal catalysts supported on carbon in low temperature nitric oxide removal is attractive due to the unique properties of activated carbon. Addition of metal catalyst however impaired the surface properties of the carbon support. Systematic investigation of hydrogen pre-treatment at 400 to 700 °C revealed significant enhancement in the chemical and physical properties leading to higher performance of CuO/EFBC in the removal of NO, especially at 600 and 700 °C. As such it helps the preparation of similar systems using carbon as support.

Introduction

The activity of nature and human such as lightning, volcano eruption and combustion of solid fuels in stationary (factories) and mobile (vehicles) sources emit nitrogen oxides (NO_x) into the atmosphere. The NO_x emission causes many adverse effects to the environment such as photochemical smog, acid rain and erosion of buildings and respiratory problems to the living beings. NO emission control can be performed by flux post-treatment such as distillation, selective catalytic reduction (SCR), non-selective catalytic reduction (SNCR), biological degradation, adsorption etc. One of the most effective technologies for reducing NO is the SCR method by titanium dioxide reacting with vanadium catalysts above 350 °C with addition of ammonia as reductant. However, this technique has many drawbacks, including high operating temperature and catalytic efficiency. Most of the efficient catalysts used in SCR are noble metals e.g. Pd, Pt, Ru [1–4] which have high catalytic activity but are relatively high in cost. This leads to extensive work being done with non-precious metals catalysts e.g. Ni, Co, Mn, Cu, La and Ce [5–10] to improve the catalytic efficiency especially for low temperature applications. Among these, copper oxide catalysts are attractive as they exhibited high catalytic removal of NO at low temperature [11] especially when using activated carbon as support. However, the nature of the catalyst catalytic activity has not been fully discovered because of the complexity of surface chemistry and pore characteristics of activated carbon. The unique properties of carbon itself is advantageous over the other supports, since the functional surface is easily modified with good mechanical resistance and easily accessible because of low cost and abundance of precursors. Interestingly, the carbon itself and metal oxides added to the system can play a role in reducing the NO emission by adsorption and NO dissociation [12, 13].

However, addition of metal catalyst impaired the surface properties of the carbon support especially the surface area and porosity as the metals were dispersed on/inside the carbon pores, blocking sites for adsorption of gases. Most studies utilizing carbon as support showed changes in the surface properties e.g. reduction in BET surface area and pore properties [5, 14–17] after addition of metal catalyst. Our preliminary work on NO removal over copper oxide supported on carbonised oil palm empty fruit bunch waste (CuO/EFBC) [18, 19] also showed significant reduction in BET surface area of the carbon support compared to fresh EFBC. As the surface properties of carbon is known to be one of important parameters affecting adsorption, such problem could degrade the adsorptive capacity, which in turn also affect dissociative NO adsorption. It is well discussed that for direct NO reduction to happen in a catalyst system supported on activated carbon, NO needs to adsorb on an activated catalyst site, which is oxygen deficient due to the reaction between the catalyst site and an unstable carbon site, generated through decomposition of carbon–oxygen complexes, followed by dissociative chemisorption of adsorbed NO by a neighbouring carbon site [20]. Interaction of these unstable oxygenated groups and their derivatives with Cu species, leading to disintegration of these groups has also been found to cause the Cu species to become mobile and form copper particles of relatively larger size and easier to be reduced [15]. Hydrogen promotion has been performed in several previous studies [21–24] and is expected to enhance NO removal in this case. The current work was conducted to systematically investigate the influence of hydrogen pre-treatment at varying temperatures from 400 to 700 °C on the activity of CuO-impregnated carbon in enhancing NO removal.

Materials and Methods

Sample Preparation

Raw oil palm empty fruit bunch (EFB) was obtained from a palm oil factory in Nibong Tebal, Malaysia. The obtained fibrous EFB sample was cleaned to remove dirt and dried for 24 h in an oven at 110°C. First, the raw EFB was modified by acid dehydration with 85% phosphoric acid (H₃PO₄) (HmBG, Germany) of 99.99% purity at 1:1 ratio of EFB to H₃PO₄ (w/v) and heated for 24 h at 400 °C in a furnace as described in our work previously [18, 19]. The addition of copper oxide (CuO) onto modified EFB carbon (EFBC) was conducted using incipient-wetness method to obtain about 5 wt% of CuO loading. During the process, the mixture of CuO and EFBC was stirred for 4–5 h, followed by double-boiling at 70 °C until the mixture

was partially dried. The mixture was then kept at 110 °C in the oven overnight to remove moisture, before being sintered in the furnace at 400 °C for 4 h. Lastly, the sample was sieved to obtain particle sizes between 300 and 600 µm and denoted as CuO/EFBC for further experiment. An elemental analysis was conducted on digested CuO/EFBC fresh sample using inductively coupled plasma–optical emission spectroscopy (ICP–OES) with Perkin Elmer Avio 500 to determine the actual concentration of copper (Cu) impregnated on the sample. The result indicates the presence of 69×10^3 mg/kg of copper on CuO/EFBC corresponding to 6.9% Cu loading.

Sample Characterisation

For characterisation of samples involving hydrogen pre-treated samples, fresh CuO/EFBC samples were initially treated in a quartz packed bed reactor with 100 mL/min of hydrogen flow at varying temperatures, i.e. 400, 500, 600 and 700 °C for an hour and then cooled to room temperature under 30 mL/min of helium flow. These resulting samples are named as H₂-400, H₂-500, H₂-600 and H₂-700 depending on the temperature used during hydrogen pre-treatment.

The investigation on Brunauer–Emmett–Teller (BET) specific surface area (S_{BET}) and pore characteristics was conducted on CuO/EFBC and H₂ pre-treated samples using nitrogen adsorption/desorption isotherms at -196 °C (Micromeritics ASAP 2020). To make a case, the S_{BET} and pore characteristics of fresh EFBC was included in the analysis. The S_{BET} was calculated from BET equation and total pore volume was attained from the N₂ adsorption isotherm at $P/P_0 = 0.95$, while pore size distribution was determined using Barrett–Joyner–Halenda (BJH) method. On the other hand, the morphological properties of CuO/EFBC and all hydrogen pre-treated samples were evaluated using Scanning Electron Microscopy with Energy Dispersive X-ray (SEM) (JEOL JSM-6460LA) at $\times 1000$ magnifications. The samples were also coated with platinum prior to the SEM-EDX analysis.

The chemical properties of fresh CuO/EFBC and all hydrogen pre-treated samples were analysed using FTIR spectroscopy (Perkin Elmer Spectrum 65 FTIR, USA) by KBr pellet method within the broad range of 450 – 4000 cm^{-1} wavelength. In addition, the average crystallite size and structure of all samples were determined by X-ray diffraction (XRD) with High Resolution X-Ray Diffractometer Bruker D8 Advance (Germany) with Cu–K α radiation (40 kV and 30 mA) in scanning angle between 10° and 90° at $0.01^\circ \text{ s}^{-1}$ scanning rate and 0.5 s step size. The average crystallite size was estimated using Scherrer Equation [25] as in Eq. (1).

$$L = \frac{K\lambda}{\beta \cos\theta} \quad (1)$$

where K is the value of the shape factor ($K=0.9$), λ is the X-ray wavelength ($\lambda=0.154$) and β represents the broadening of peak at half width or FWHM (full width half maximum) in radians.

To evaluate the reducibility of all samples, a hydrogen-temperature programmed reduction (H₂-TPR) was conducted using chemisorption analyser (Micromeritics Chemisorb 2720 TPx). Prior to the analysis, 0.025 g of sample was pre-treated at 300 °C for one hour under flow of 99.99% helium at 20 mL/min in order to remove moisture and impurities of adsorbates. The H₂-TPR profile was determined at increasing temperature of 10 °C/min, under flow of 20 mL/min 10% (vol.) H₂/Ar.

In addition, the surface basicity and acidity of all samples were investigated using carbon dioxide and ammonia-temperature programmed desorption (CO₂-TPD and NH₃-TPD) respectively using the same chemisorption analyser. Prior to analysis, 0.035 g of sample was pre-treated at 600 °C with 30 mL/min argon flow for an hour and then cooled to room temperature under 20 mL/min helium flow for half an hour. The CuO/EFBC was first saturated with either CO₂ or NH₃ by passing through purified CO₂ or 5% (vol.) NH₃/Ar at 20 mL/min for 30 min for CO₂-TPD or NH₃-TPD analysis respectively.

NO Breakthrough Study

The influence of hydrogen pre-treatment on NO removal was studied by varying the pre-treatment temperature from 400 to 700 °C under flow of 100 mL/min H₂ for 1 h, each subsequently followed by a 2-h NO breakthrough experiment at 100°C using a packed bed reactor made of quartz cylinder, heated in a tubular furnace (Vecstar, UK). The reactor was connected to the gas cylinders (30% H₂/N₂, 0.3% NO/He and He provided by Linde, Malaysia) using PFA tubing fitted with Swagelok fittings, while gas flow was controlled by Aalborg mass flow controllers. The operating parameters e.g. CuO/EFBC bed thickness, initial concentration of NO and total gas flowrate were kept constant at 1 cm, 500 ppm and 100 mL/min respectively. The NO concentrations from inlet bypass and analyser outlet were measured by a NO–NO₂ analyser (TESTO 340, Germany).

The NO adsorption capacity was obtained by integrating the fraction of NO removal ($1 - C/C_0$) per minute by the trapezoidal method [24, 25] as discussed elsewhere [19] and shown in Eq. 2 below:

$$q = \frac{C_{NO} Q_f t_f y_f}{m_c} \quad (2)$$

where q is adsorption capacity of NO (mg/g), C_{NO} is NO concentration (mg/L), Q_f is the flow rate of NO, t_f is the time equivalent in minutes obtained by integrating the fraction of NO removed at time t as shown in Eq. 3, y_f is the mole fraction of NO concentration and m_c is mass of adsorbent (g).

$$t_f = \int_0^\infty 1 - \frac{C}{C_0} \quad (3)$$

Results and Discussion

Characterisation of CuO/EFBC and H₂ Pre-treated Samples

Surface Area and Pore Analysis

Surface area and pore analysis was conducted on all samples including fresh EFBC to corroborate the effects brought about by CuO impregnation and H₂ pre-treatment at different temperatures on the physical properties of CuO/EFBC. Figure 1a compares the N₂ adsorption/desorption isotherms of fresh EFBC and CuO/EFBC, while Fig. 1(b) depicts the isotherms of CuO/EFBC and all H₂ pre-treated samples (H₂-400, H₂-500, H₂-600 and H₂-700). All samples feature isotherm curves with a hysteresis loop at the higher relative pressure region, which is characteristic of Type IV isotherm, indicating an indefinite multilayer formation followed by pore condensation of the capillaries, normally found on multi porous surfaces i.e. micropores, mesopores, macropores, and on the external surface [26, 27] once a monolayer coverage is completed at low P/P₀. Except for EFBC which is a classic example of Type IV isotherm, the others seem to be missing the final saturation plateau which is another typical feature of Type IV. This indicates that the isotherms may be a composite of Type IV and Type II, which is characterized by indefinite sorption at maximum P/P₀ normally attributed by physisorption of gases on nonporous or macroporous adsorbent [28]. The more gradual changes seen at the beginning of multilayer adsorption especially in samples pre-treated at higher temperatures of 500, 600 and 700 °C indicate a significant overlap of the monolayer coverage and the onset of multilayer adsorption.

In addition, the hysteresis loops of CuO/EFBC (although not obvious in Fig. 1 due to the lower vertical magnitude of its curve compared to the others) and H₂-400 with a characteristic desorption shoulder are of H3 type, which has also been referred to samples having pseudo-Type II character associated with the metastability of adsorption fluid and

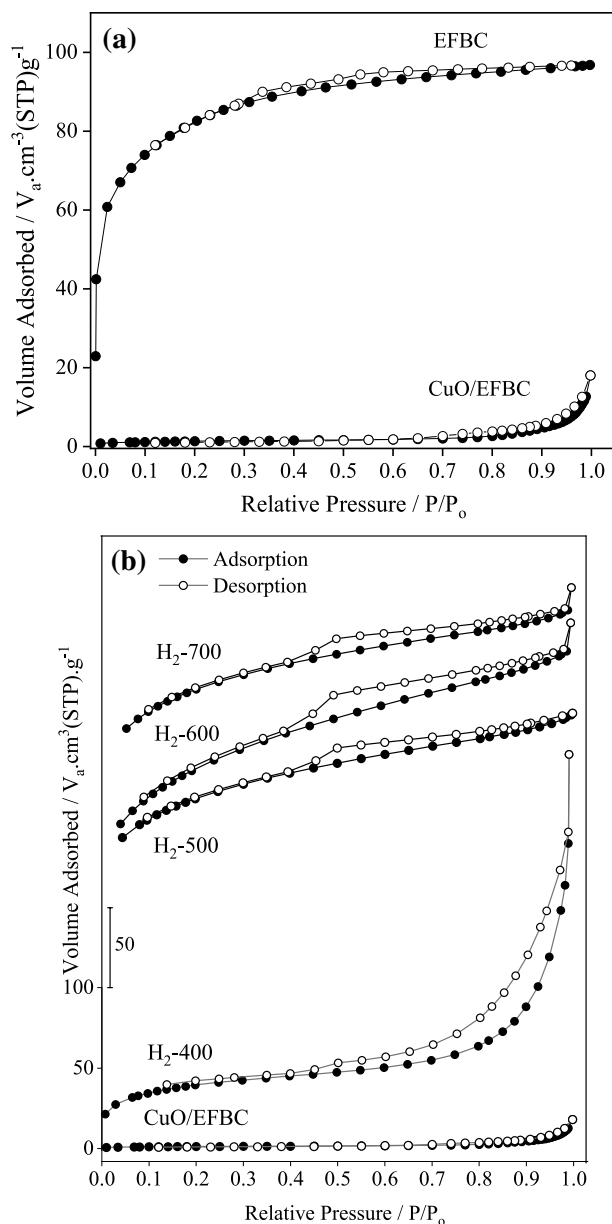


Fig. 1 Nitrogen adsorption/desorption of **a** fresh EFBC and CuO/EFBC; **b** fresh CuO/EFBC and H₂ pre-treated samples

delayed capillary condensation attributed to the low degree of pore curvature and non-rigidity of the adsorbents [29]. On the other hand, the hysteresis loops of CuO/EFBC samples at higher H₂ pre-treatment temperatures (H₂-500, H₂-600 and H₂-700) are more of H4 type, which could be equivalent to an H3 loop on the relatively small non-microporous part of the adsorbent [29]. In addition, the H₂ pre-treated samples can be observed to have an open hysteresis loop at low relative pressures, possibly due to limitations in nitrogen diffusion into the narrow micropores of the adsorbent [30].

Table 1 summarizes the BET specific surface area (S_{BET}), total pore volume and average pore diameter of fresh EFBC,

CuO/EFBC and H₂ pre-treated samples. As mentioned earlier, CuO impregnation has indeed lowered the S_{BET} of EFBC from an initial value of 215 to around 4.81 m²/g, total pore volume from around 0.15 to 0.018 cm³/g, micropore volume from 0.147 to 0.0002 cm³/g and micropore ratio from 98.10 to 1.18%. The average pore diameter is also enlarged from narrow (2.78 nm) to larger mesopores (14.92 nm). Subjecting CuO/EFBC to H₂ pre-treatment at different temperatures from 400 to 700 °C raises the S_{BET} of CuO/EFBC to 516 m²/g, which is more than double the initial S_{BET} of CuO/EFBC and enhances the micropore volume, total pore volume and micropore ratio to 0.126 cm³/g, 0.34 cm³/g and 36.93% respectively. It is important to note that for H₂-400, the S_{BET} and micropore volume are still much smaller (160 m²/g and 0.025 cm³/g respectively), while the average pore diameter is still larger (5.69 nm) compared to the fresh EFBC samples. H₂ pre-treatment at higher temperatures between 500 and 700 °C restores the average pore diameter to ca. 2.6 nm, which is more favourable for NO adsorption because the diameters of gas molecules are usually small, around 0.4 to 0.9 nm. The observed changes in

the pore properties of CuO/EFBC due to H₂ pre-treatment are initially quite significant at lower temperature (400 °C), but then become more gradual from 500 °C onwards. In addition, the pore size distribution (PSD) determined by BJH method (Fig. 2) shows that while the pore size of CuO/EFBC and H₂ pre-treated samples is widely distributed from 2 nm (wider micropore) to 250 nm (macropore region), the pores are predominantly concentrated within the smaller sized pore region with diameter around 2–5 nm. The wide distribution of pore sizes in H₂-pre-treated samples could be one of the reasons for the observed changes in hysteresis loop from H3 to H4 at higher H₂ pre-treatment temperatures.

Surface Morphology and Elemental Analysis

The SEM images of fresh CuO/EFBC and H₂ pre-treated samples of different temperatures (400, 500, 600 and 700 °C) are presented in Fig. 3a–e respectively at 1000x magnifications. As can be observed in Fig. 3a, the external surface of fresh CuO/EFBC shows irregular pore structure with flaky attachment of carbon particles, while the hydrogen pre-treated samples in Fig. 3b–e show more uniform and well-developed pores, especially at 700 °C, indicating possible constitution of a new matrix has happened during the H₂ pre-treatment stage [31]. The well-defined pore formation seen in Fig. 3b–e is in good agreement with the high surface area reported earlier in with the increase in H₂ pre-treatment temperature. The atomic percentage (at%) of several key surface elements (carbon, oxygen, phosphorus and copper) obtained from EDX analysis is shown in Table 2. In general, the fraction of O and P (coming from phosphoric acid activation) on the carbon surface reduces from around 21.36 to 11.83 at% and from 18.00 to 4.93 at% respectively, perhaps due to the decomposition of the surface functional groups containing O and P when pre-treated with H₂ at elevated temperatures. In correspondence to that, the fraction of carbon increases from 54.60 to 77.80 at% while the fraction of Cu slightly reduces from 6.04 to 5.43 at% at 700 °C. In between the 400 and 700 °C, some fluctuations occur especially on the fraction of P possibly due to irregularities in the sampling point during SEM analysis on the different samples.

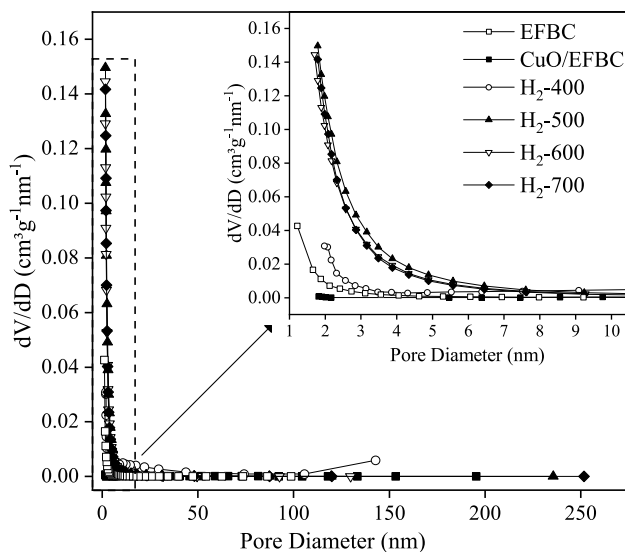


Fig. 2 Pore diameter distribution (PSD) of fresh CuO/EFBC and H₂ pre-treated samples

Table 1 Surface area and pore characteristics of fresh EFBC, CuO/EFBC and H₂ pre-treated samples

Sample	Surface area (m ² /g)	Micropore volume (cm ³ /g)	Total pore volume (cm ³ /g)	Micropore ratio (%)	Average pore diameter (nm)
EFBC	215.0	0.1470	0.1500	98.10	2.780
CuO/EFBC	4.814	0.0002120	0.01796	1.180	14.92
H ₂ -400	159.5	0.02462	0.2270	10.85	5.693
H ₂ -500	466.3	0.08537	0.3299	25.87	2.830
H ₂ -600	448.0	0.09715	0.2911	33.37	2.599
H ₂ -700	516.4	0.1257	0.3405	36.93	2.637

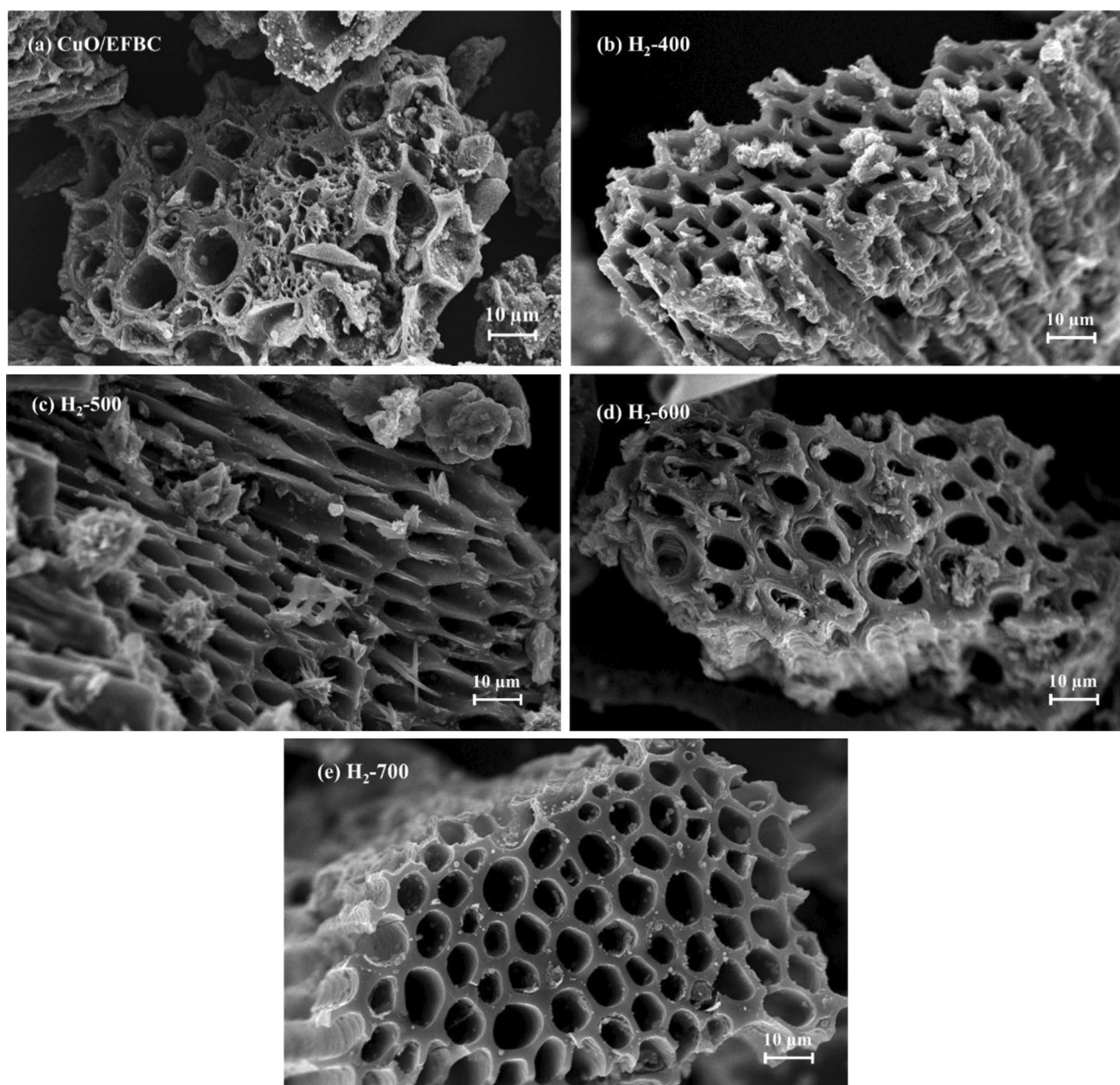


Fig. 3 SEM images of fresh CuO/EFBC and H₂ pre-treated samples

Table 2 Elemental analysis using EDX for fresh CuO/EFBC and H₂ pre-treated samples

Sample	Surface element (at%)			
	C	O	P	Cu
CuO/EFBC	54.60	21.36	18.00	6.04
H ₂ -400	62.56	21.45	11.98	4.00
H ₂ -500	64.60	24.60	7.090	3.71
H ₂ -600	64.22	19.24	12.55	3.99
H ₂ -700	77.80	11.83	4.930	5.43

Surface Functional Groups

The FTIR spectra of all samples in Fig. 4 show the presence of a broad curve between 3700 and 3200 cm⁻¹ with a distinctive peak around 3430 cm⁻¹, indicative of O–H bonds (hydroxyl and phenolic groups) [31, 32]. On the other hand, two minor peaks observed between 2930 and 2900 cm⁻¹ denote the presence of alkanes and alkyls with possible C–H (stretching) in all samples. These peaks are sharper in H₂-600 and H₂-700 samples, possibly due to their higher intensity at elevated temperatures. In addition, a broad,

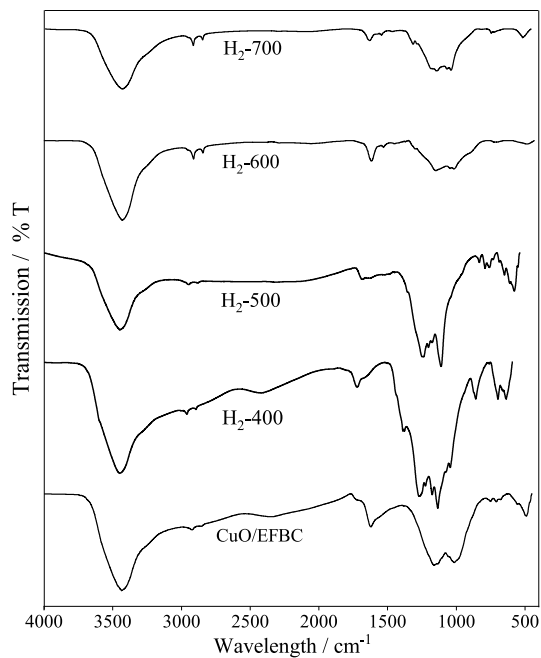


Fig. 4 FTIR spectra for fresh CuO/EFBC and H₂ pre-treated samples

shallow peak also appears around 2400–2300 cm⁻¹ in CuO/EFBC and H₂-400 spectra, which can be ascribed to weak bond of nitrile or alkyne with possible C≡N (stretching). This peak is noted to be absent from the spectra of H₂-500, H₂-600 and H₂-700 samples. Similarly, the peak within 1720 to 1706 cm⁻¹, which can be assigned to carboxylic acid (C=OOH) is also missing from H₂-600 and H₂-700. In contrast, the spectra of H₂-600 and H₂-700 samples display peaks around 1624 and 1621 cm⁻¹ which can be attributed to C=O conjugated groups and aromatic rings [31].

Of particular importance are the peaks within 1300 and 800 cm⁻¹, which centre most of the acidic oxygenated groups and vary quite significantly among the H₂ pre-treated samples at low (400 and 500 °C) and high (600 and 700 °C) temperatures. The peaks around 1250–1150 cm⁻¹ generally attributed to oxidized carbons with lactones, carboxyls and/or phenolic group can be seen to be more pronounced in the H₂-400 and H₂-500 spectra rather than in fresh CuO/EFBC, H₂-600 and H₂-700. Other than that, the peak that appears at 1220 cm⁻¹ in all samples (with sharper peak on H₂-400 and H₂-500 spectra) can be attributed to phosphorus containing groups e.g. polyphosphates or phosphates, while the narrow peak at 1050 cm⁻¹ that appears only on the H₂-400 and H₂-500 spectra can be assigned to lactone and quinone groups. A small vibration that exists below 900 cm⁻¹ in CuO/EFBC and more pronounced in H₂-400 and H₂-500 is indicative of aromatic rings with possible C–H bending. Below 700 cm⁻¹, the peaks that appear around 660 cm⁻¹ and 530 cm⁻¹ could be assigned to Cu–O stretching, an indication of the presence of CuO in the samples [32, 33].

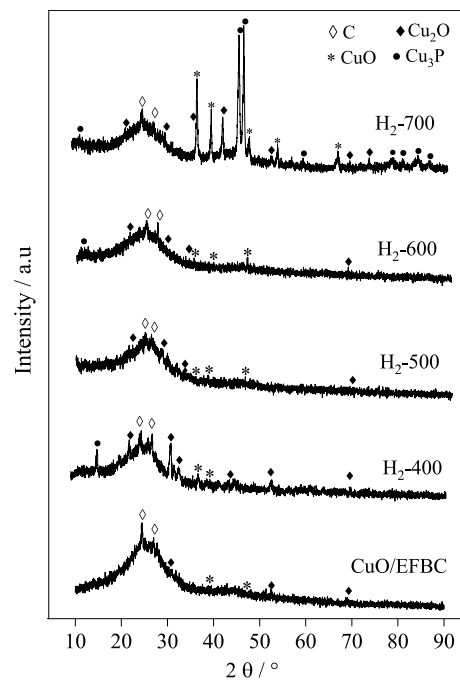


Fig. 5 X-ray diffractograms for fresh CuO/EFBC and H₂ pre-treated samples

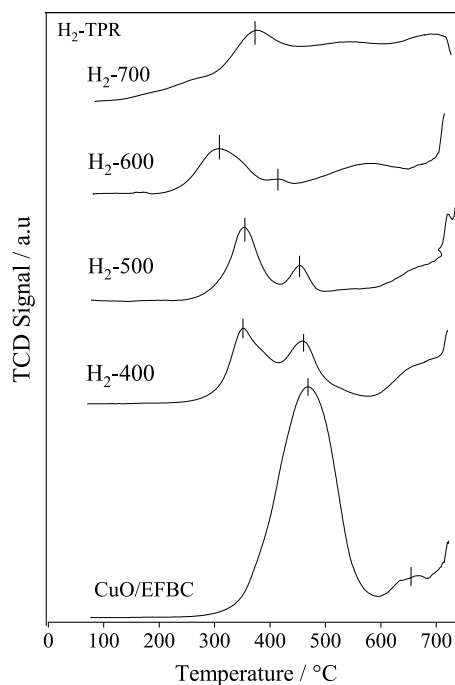
The FTIR spectra of both fresh CuO/EFBC and H₂ pre-treated samples confirm the presence of acidic oxygen functional groups (carboxylic groups and their derivatives), with more pronounced peak intensity of these groups being observed on H₂-400 and H₂-500 samples. Some of the surface oxygenated groups are missing from samples pre-treated at elevated temperatures especially H₂-600 and H₂-700, due to the reducing hydrogen and thermal decomposition. The oxygenated surface groups observed on the surface of the samples are in O–C vibration of C–O, C=O, COOH and C–O–P, due to the phosphoric acid activation of the precursor material. It has been well accepted that the presence of these oxygenated groups is essential as they are unstable O–C groups which can be easily decomposed and bound to reduced Cu species, especially when no external reductant is supplied. The presence of Cu–O derived species is also evidenced with significant intensity on the FTIR spectra of H₂-400 and H₂-500, which are also discovered to be predominated by oxygenated surface groups. Wang et al. [34, 35] also reported that the presence of oxygenated surface groups did not only reduce the temperature of Cu²⁺ reduction, but also induced high dispersion of copper. On the other hand, H₂-600 and H₂-700 are populated by more basic surface groups in the form of aldehydes, alkanes, alkyls and aromatic rings.

Table 3 Crystallite size and structure for fresh CuO/EFBC and H₂ pre-treated samples

Sample	Crystallite size (nm)	Crystallite structure
CuO/EFBC	41.06	Triclinic
H ₂ -400	48.89	Monoclinic
H ₂ -500	59.57	Monoclinic
H ₂ -600	56.12	Monoclinic
H ₂ -700	24.89	Hexagonal

Crystallite Size and Structure

Figure 5 shows the X-ray diffractograms while Table 3 shows the crystallite size and structure of CuO/EFBC and H₂ pre-treated samples. A good agreement between the experimental diffraction angle (2θ) and standard diffraction angle (2θ) was observed using the standard powder diffraction cards (JCPDS). The XRD patterns can be seen to change with increasing H₂ pre-treatment temperature. At 400, 500 and 600 °C, there are many ill-defined peaks which cannot be easily distinguished, while at 700 °C, the peaks become sharper, indicating higher degree of crystallinity. The broad peak around $2\theta = 20^\circ\text{--}30^\circ$ and a broad hump within $40^\circ\text{--}50^\circ$ that appear in all samples can be assigned to the plane reflection of (002) and (100) due to the presence of amorphous carbon with carbon ring disorderly piled up or agglomerated [36, 37]. The intensity of the peaks is slightly increased as H₂ pre-treatment temperature increases from 400 to 700 °C, in agreement with the rise in carbon percentage determined in EDX analysis. These peaks indicate the presence of some degree of micro crystallinity with turbostratic graphite in the samples. The increase in the background signal between peaks at 10 and 20° could also be attributed to the presence of micropores in the samples, which could scatter the X-ray beam, causing the increase in background signal [38]. In addition, the peaks of CuO, Cu₂O and Cu₃P can also be identified from the XRD patterns. Based on JCPDS card of 00-001-1117, peaks that appear around $2\theta = 35.74^\circ$ (– 111), 38.96° (111), 49.21° (– 202), 53.89° (020) and 68.43° (220) correspond to the primary reflection phases of CuO [39–41], while in accordance to JCPDS card of 00-005-0667, peaks that appear at $2\theta = 35.42^\circ$ (111), 42.30° (200), 52.46° (211), 69.57° (310) and 73.53° (311) refer to CuO [15, 42, 43] and Cu⁰ [39, 43]. On the other hand, peaks that appear around $2\theta = 45.09^\circ$ (300), 46.15° (113), 47.29° (212), 59.01° (222), 78.27° (314) and 80.64° (006) can be assigned to copper phosphide (Cu₃P) based on JCPDS card: 01-071-2261 [44], thus confirm the presence of chemical interaction between Cu and P groups. The identified copper compounds i.e. copper oxide, cuprite and copper phosphide are essentially active sites that could play a significant role in the removal of NO.

**Fig. 6** H₂-TPR profile of fresh CuO/EFBC and H₂ pre-treated samples

The average crystallite size along the layer planes, L_a obtained by using Scherrer Equation is summarized in Table 3. As can be seen in Table 3, samples pre-treated at lower temperatures (400 and 500 °C) show average crystallite sizes of approximately 48.89 and 59.57 nm respectively, higher than fresh CuO/EFBC's crystallite size (41.06 nm), while with higher pre-treatment temperatures (600 and 700 °C), the average crystallite sizes of the samples are reduced to 56.12 and 24.89 nm respectively. In addition, H₂ pre-treatment at the different temperatures also affects the crystal structure of the samples. Fresh CuO/EFBC exhibits triclinic crystal structure which then changes to monoclinic when pre-treated with H₂ at 400–600 °C and to hexagonal when pre-treated at 700 °C.

Temperature Program Reduction (TPR)

Figure 6 shows the H₂-TPR profile of fresh CuO/EFBC and H₂ pre-treated samples within 50 to 750 °C. As can be observed, fresh CuO/EFBC has a prominent, broad peak of H₂ consumption within temperatures of 300–600 °C (with peak maximum at 467 °C) and another small peak around 650 °C, indicating that the carbonised sample is reducible within the temperature range. The peak at lower temperatures may be attributed to reduction of surface active sites of weaker strength including reduction of Cu²⁺ (CuO) to Cu⁺ (Cu₂O) while the second peak may be ascribed to reduction of stronger surface active sites and consecutive reduction

of Cu^+ (Cu_2O) to Cu^0 (metallic Cu) or direct reduction of Cu^{2+} to Cu^0 [42, 45]. The non-supported reduction of CuO species to Cu^0 is recognised as a one-step process that peaks at about 250 °C [46]. Therefore, the observed higher reduction temperature of CuO/EFBC indicates the presence of strong chemical interaction of support and surface actives sites including Cu, in addition to its dependence on copper dispersion and the nature of support behaviour [42, 47].

When CuO/EFBC was pre-treated with H_2 at the different temperatures, H_2 consumption peak in TPR profile shrinks and shifts to lower temperatures around 300–350 °C (first peak) and within 400–465 (second peak) because of the decrease in the surface sites available to adsorb H_2 as the samples has been subjected to H_2 pre-treatment beforehand. In addition, lower amount of H_2 consumption is required for reduction of H_2 pre-treated samples, fluctuating around 0.3–0.8 mmol/g compared to fresh CuO/EFBC (2.001 mmol/g).

Temperature Programmed Desorption (TPD)

The chemical properties of the surface functional groups available on CuO/EFBC and H_2 pre-treated samples were evaluated through carbon dioxide and ammonia temperature programmed desorption (CO_2 -TPD and NH_3 -TPD). In general, samples with strong adsorption bonds give rise to higher desorption peaks in TPD whereas the desorption temperature and the peak area (under the curve) represent the strength and the intensity of basic or acidic sites respectively

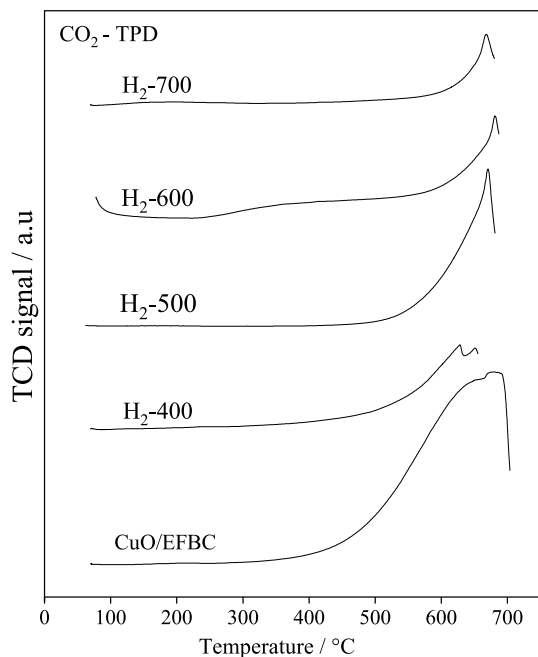


Fig. 7 CO_2 -TPD profile for fresh CuO/EFBC and H_2 pre-treated samples

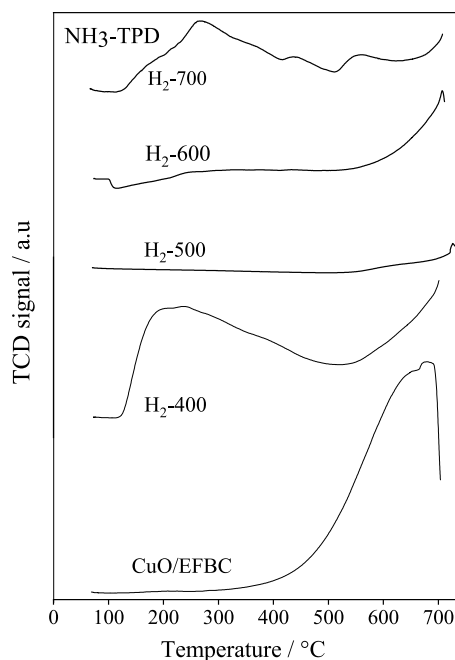


Fig. 8 NH_3 -TPD profile for fresh CuO/EFBC and H_2 pre-treated samples

[48–51]. Based on the CO_2 -TPD and NH_3 -TPD profiles in Figs. 7 and 8 respectively, CuO/EFBC and all H_2 pre-treated samples can be observed to have both basic and acidic sites at different strength and intensity. However, it is unfortunate that the intensity of the desorption peaks which are located at temperatures beyond the tested region (50–700 °C), cannot be fully quantified to differentiate the number of basic and acidic sites among the different samples.

In CO_2 -TPD profile of fresh CuO/EFBC, a CO_2 desorption peak can be initially seen to appear around 450 °C, with peak maximum at temperature higher than 600 °C. In H_2 pre-treated samples, the onset temperature of the CO_2 desorption peak increases from 500 to 600 °C with increasing pre-treatment temperatures from 400 to 700 °C, suggesting that the temperature rise promotes stronger surface basicity in the samples [44, 53]. This is in line with the decomposition of some acidic oxygenated sites observed in FTIR spectra at elevated temperatures, giving rise to the presence of more basic groups. Based on what is measurable below 700 °C, the CO_2 uptake for fresh CuO/EFBC ca. 983 $\mu\text{mol/g}$ is found to be higher than that observed for H_2 pre-treated samples, which fluctuates from 9 (H_2 -400) to 378 (H_2 -500), 28 (H_2 -600) and 89 $\mu\text{mol/g}$ (H_2 -700) at the different pre-treatment temperatures. However, as mentioned earlier, these peaks are incomplete and cannot represent the actual intensity of surface basic sites within the temperature studied.

On the other hand, Fig. 8 shows the appearance of an NH_3 desorption peak at 400 °C (with peak maximum around 650 °C), indicating the presence of strong acid sites in fresh

CuO/EFBC. When pre-treated at 400 °C under H₂ flow, two NH₃ desorption peaks appear on the TPD profile, one at a lower temperature of 125 °C (which peaks around 225 °C) and the other at 550 °C, indicating that H₂ pre-treatment at 400 °C could induce generation of both weak and strong acid sites in CuO/EFBC [52]. Apparently, the weaker acidic sites could be removed by an increase in H₂ pre-treatment temperatures to 500 and 600 °C as such peaks are no longer observed on the two samples (H₂-500 and H₂-600) within the lower temperature region (less than 400 °C). Other than that, both samples still exhibit a desorption peak at high temperature (above 600 °C) indicative of strong acidic sites. Further increase in the H₂ pre-treatment temperature to 700 °C regenerates the weak acidic sites which can be seen to appear at similar temperature of 125 °C (but peaks at 270 °C) on H₂-700 TPD profile, in addition to the stronger acid sites seen in tiny peaks around 420 and 500 °C. Based on the measurable NH₃ uptake below 700 °C, H₂-400 appear to have highest surface acidity (1077 μmol/g), followed by H₂-700 (291 μmol/g), CuO/EFBC (119 μmol/g), H₂-600 (12 μmol/g) and H₂-500 (1 μmol/g). As these values are based on incomplete peaks, the trend does not explicitly represent the actual surface acid intensities on the different samples.

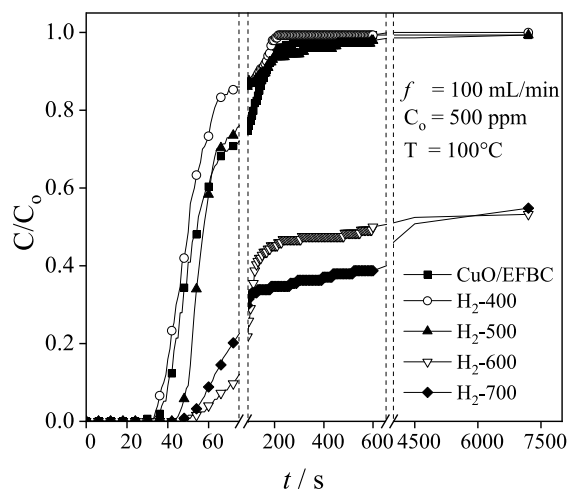


Fig. 9 NO breakthrough curves of fresh CuO/EFBC and H₂ pre-treated samples

Table 4 Breakthrough time (at $C/C_0 = 0.05$), saturation time (at $C/C_0 = 0.95$) and NO adsorption capacity at $C/C_0 = 0.5$ and 0.95 for the different samples

Sample	Breakthrough time $C/C = 0.05$ (s)	Saturation time at $C/C_0 = 0.95$ (s)	Adsorption capacity at $C/C_0 = 0.5$ (mg/g)	Adsorption capacity at $C/C_0 = 0.95$ (mg/g)
CuO/EFBC	31	203	1.23	1.65
H ₂ -400	38	159	1.41	1.57
H ₂ -500	51	598	1.89	5.67
H ₂ -600	60	–	41.01	–
H ₂ -700	62	–	62.74	–

NO Breakthrough Study on CuO/EFBC and H₂ Pre-treated Sample

The influence of H₂ pre-treatment at different temperatures on NO removal was evaluated by changes in breakthrough time (at $C/C_0 = 0.05$), saturation time (at $C/C_0 = 0.95$) and NO adsorption capacity. Figure 9 shows that within 40 s of the breakthrough experiment, all samples initially achieved 100% NO removal, but this soon starts to decrease. Hydrogen pre-treatment appears to have little influence on breakthrough time especially with pre-treatment temperatures less than 600 °C, as all samples reach breakthrough within 65 s (as listed in Table 4) possibly due to the use of thin bed depth in all breakthrough experiments. NO removal of CuO/EFBC and H₂-400 achieves bed saturation ($C/C_0 = 0.95$) within 200 s (3 min), while the increase in H₂ pre-treatment temperatures to 500 °C prolongs the saturation time to 600 s. Further increase in the H₂ pre-treatment temperature to 600 and 700 °C remarkably increases the stability of NO removal as the adsorbent beds have not reached saturation even after more than 2 h of experiment. The NO adsorption capacities achieved at $C/C_0 = 0.95$ are 1.65, 1.57 and 5.67 mg/g for CuO/EFBC and H₂ pre-treated samples at lower temperatures i.e. H₂-400 and H₂-500 respectively. The H₂-600 and H₂-700 samples show superior performance in NO removal, with NO adsorption capacity of 41.01 and 62.74 mg/g respectively at $C/C_0 = 0.50$. In a previous work, activated carbon prepared from sawdust, modified with 10% metal catalysts i.e. K, Cu, Fe and Ni were found to produce NO adsorption capacity of 38.80, 34.66, 20.56 and 27.43 mg/g respectively under 500 mL/min flow of 10⁻³ NO, 5 vol% O₂ at 298K [53, 54].

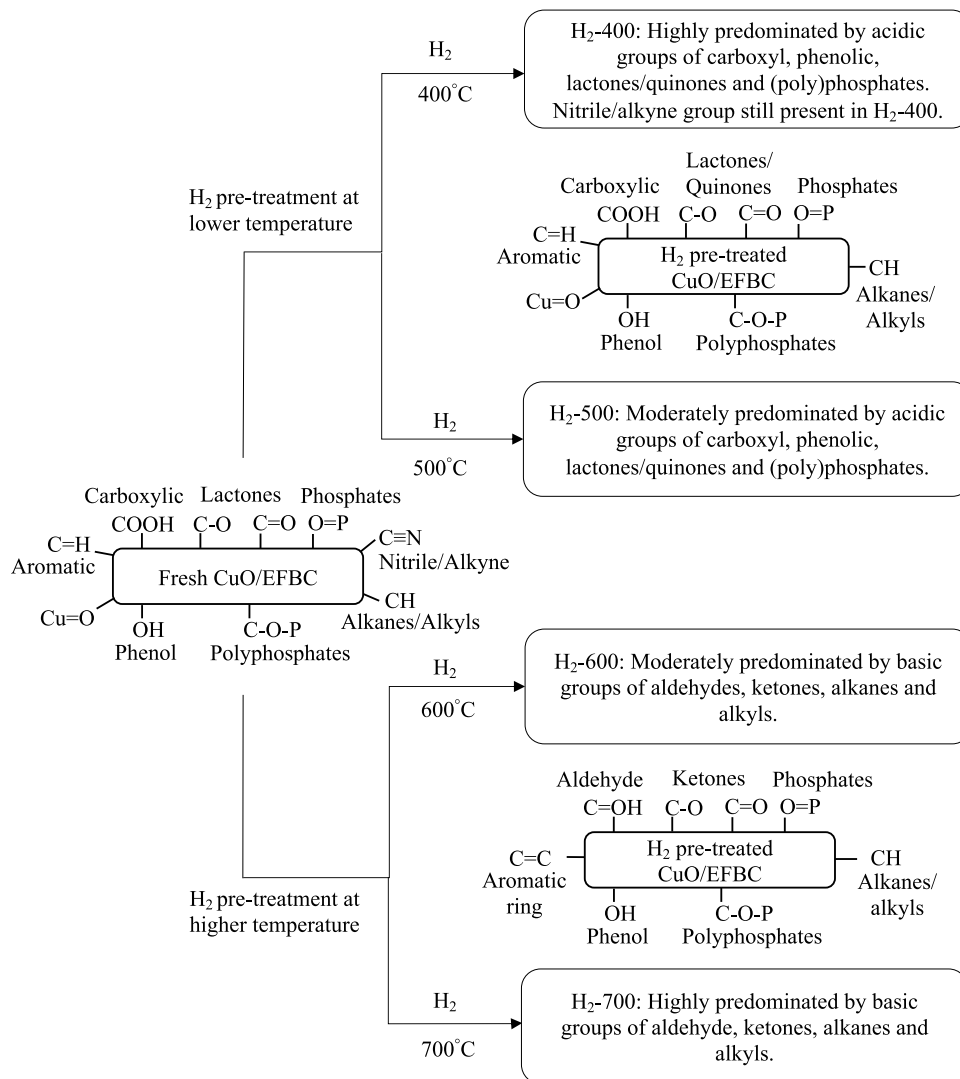
In general, it can be observed that NO removal has a positive relationship with the H₂ pre-treatment temperature. Possible direct explanation is that the rise in H₂ pre-treatment temperature have simply enhanced the active sites available on the catalyst/carbon. This however may be accomplished by several ways, e.g. by removing acidic oxygenated surface groups on the carbon support and thus enhance the carbon surface properties catalytically and also physically (through enhancement in the surface area and pore properties) which are imperative for NO adsorption and/or also modifying

the copper species to be in oxidation states which are more favourable for dissociative NO adsorption and reduction [55–57].

Apparently, the role of H₂ pre-treatment temperatures in NO removal is not as simple as expected and is a function of both changes in the surface chemical and the physical properties of CuO/EFBC. The increase in surface area and pore of volume undoubtedly would result in increasing NO removal efficiency [58], while decomposition of acidic oxygen functional groups at elevated temperatures has been reported to increase the basicity of the carbon surface in various studies [59–61]. As NO species is known to be acidic, it is expected that the presence of these basic active sites will be able to play a significant role in increasing NO adsorption onto the carbon surface, accompanied by NO dissociation into nitrogen. A schematic representation of acidic and basic groups at the different pre-treatment temperatures is shown in Fig. 10. Based on the FTIR and NH₃-TPD results discussed

earlier, H₂ pre-treatment of CuO/EFBC at low temperatures (400 and 500 °C) is found to enhance predomination of acidic oxygenated surface groups (e.g. carboxy, lactone/quinone and phenolic groups). This causes the NO removal of H₂-400 to reduce although the S_{BET} and pore properties (higher pore volume and smaller pore size) are quite significantly enhanced. At 500 °C, some of these weak acid sites populating the adsorption surface are decomposed, while the basicity of the sample, surface area and pore properties are enhanced, leading to higher NO removal. More of these acidic groups are decomposed at 600 and 700 °C, while the H₂-600 and H₂-700 samples become more significantly predominated by basic groups, such as aldehyde, alkanes, alkyls and aromatic groups, in accordance with the increase in the strength of surface basicity observed in CO₂-TPD profile. The dependence of surface acidic site decomposition on temperature has also been reported by several previous studies, showing that weakly acidic groups (such as carboxylic, anhydrides

Fig. 10 Schematic representation of surface groups available at different H₂ pre-treatment temperatures



and lactones) decompose at lower temperatures, while the strongly acidic groups (such as carbonyl, phenol and quinone) decompose at higher temperatures up to 980 °C [60, 61]. The decomposition of these acidic oxygen-containing groups on the carbon surface during H₂ pre-treatment at elevated temperature, will lead to the presence of unsaturated carbons that could react with H₂, exhibiting stable basic sites which would be available to NO dissociation from gaseous molecules. In the case reported by Radovic et al. for selective oxidation of CO, pure AC was able to form superoxide species after pre-treatment with H₂ at temperatures higher than 350 °C, while in the presence of Ag catalyst, the superoxide species were more easily generated after pre-treatment with H₂ at lower temperature of 200 °C [62].

It is also worth to note that phosphorus containing groups are predominant on samples pre-treated with H₂ at 400 and 500 °C, but decreases on samples pre-treated with H₂ at 600 and 700 °C. On the other hand, Wang et al. showed in their case that heat treatment at 400–500 °C in the presence of hydrogen already caused a remarkable decrease in phosphorus-containing groups in concomitant with the decrease in oxygen groups from the carbon surface [24], generating more unstable carbon sites which could then bind to Cu catalyst and react with NO.

In addition, the presence of different Cu valences on the carbon support also plays an important role in NO removal. Previous work showed that CuO (Cu²⁺) and Cu₂O (Cu⁺) are more favourable for NO reduction [5], however, the Cu₂O (Cu⁺) as well as metallic Cu (Cu⁰) was found to hamper NO reduction over CuO/AC catalysts in the presence of nitric acid [63]. The change in the valences is well known to be controlled by calcination temperature, with lower valence of copper species formed on AC at higher calcination temperature [5, 64]. In this work, copper was calcined at 400 °C, thus CuO (Cu²⁺) and Cu₂O (Cu⁺) species are expected to be predominant, however with H₂ pre-treatment temperature being increased to 700 °C, it is possible that the presence of more lower valence species could be expected. However, based on the XRD diffractograms showed earlier, copper species of both high and lower valences (CuO, Cu₂O and Cu₃P) are found to be predominant in all H₂ pre-treated samples, especially in H₂-700. Therefore, it can be assumed that the influence of copper valency on dissociative NO removal is not significantly different among the H₂ pre-treated samples. Other than that, the smaller crystallite size exhibited by samples pre-treated at higher temperatures (600 and 700 °C) could also be beneficial for NO removal efficiency. In a previous work done by Dong et al. [65] larger CeO₂ and CuO crystallite size was found to reduce CuO dispersion and subsequently inhibited CO conversion.

Conclusions

The study investigates the influence of hydrogen pre-treatment at different temperatures on low-temperature nitric oxide removal by oil palm empty fruit bunch activated carbon prepared by modification with phosphoric acid dehydration, followed by copper oxide impregnation using incipient-wetness method (CuO/EFBC). Based on characterisation of fresh and H₂ pre-treated samples at 400, 500, 600 and 700 °C, it was found that H₂ pre-treatment mainly affects the presence of acidic oxygenated groups and the physical properties e.g. BET surface area and pore characteristics of CuO/EFBC as well as CuO crystallite size and structure. At lower H₂ pre-treatment temperature (400 °C), the surface is mainly predominated by acidic oxygenated groups which are decomposed at higher pre-treatment temperatures depending on their strength, leading to generation of more basic sites which are favourable for acidic NO removal. Better surface area and more developed pore characteristics (higher pore volume and smaller pore size) and smaller average crystallite size also contribute to better NO removal, especially at high pre-treatment temperatures, i.e. 600 and 700 °C.

Acknowledgements The authors would like to thank the Ministry of Higher Education Malaysia for financial support through Fundamental Research Grant Scheme (FRGS) under a Grant Number of FRGS/2/2013/SG01/UNIMAP/02/1. We would also like to thank Dr Tuan Amran Tuan Abdullah and Dr Walid Nabgan for TPR and TPD measurements.

References

1. Bosch, H., Janssen, F.: Catalyst testing. *Catal. Today* **2**, 403–431 (1988)
2. Khosravi, M., Sola, C., Abedi, A., Hayes, R.E., Epling, W.S., Votsmeier, M.: Oxidation and selective catalytic reduction of NO by propene over Pt and Pt/Pd diesel oxidation catalysts. *Appl. Catal. B* **147**, 264–274 (2014)
3. Tanaka, T., Okuhara, T., Misono, M.: Intermediacy of organic nitro and nitrite surface species in selective reduction of nitrogen monoxide by propene in the presence of excess oxygen over silica-supported platinum. *Appl. Catal. B* **4**, L9 (1994)
4. Wang, L., Chen, H., Yuan, M.H., Rivillon, S., Klingenberg, E.H., Li, J.X., Yang, R.T.: Selective catalytic reduction of nitric oxide by hydrogen over Zn-ZSM5 and Pd and Pd/Ru based catalysts. *Appl. Catal. B* **152–153**, 162–171 (2014)
5. Chuang, K.H., Liu, Z.S., Wey, M.Y.: Catalytic activity of copper-supported catalyst for NO reduction in the presence of oxygen: fitting of calcination temperature and copper loading. *Mater. Sci. Eng. B* **175**, 100–107 (2010)
6. Wang, X., Wen, W., Mi, J., Li, X., Wang, R.: The ordered mesoporous transition metal oxides for selective catalytic reduction of NOx at low temperature. *Appl. Catal. B* **176–177**, 454–463 (2015)
7. Grzybek, T., Klinik, J., Dutka, B., Papp, H., Suprun, V.: Reduction of N₂O over carbon fibers promoted with transition metal oxides/hydroxides. *Catal. Today* **101**, 93–107 (2005)

8. Kante, K., Deliyanni, E., Bandosz, T.J.: Interactions of NO₂ with activated carbons modified with cerium, lanthanum and sodium chlorides. *J. Hazard. Mater.* **165**, 704–713 (2009)
9. Abdedayem, A., Guiza, M., Ouederni, A.: Copper supported on porous activated carbon obtained by wetness impregnation: Effect of preparation conditions on the ozonation catalysts characteristics. *C. R. Chim.* **18**, 100–109 (2015)
10. Lu, C.Y., Rau, J.Y., Chen, J.C., Huang, S.T., Wey, M.Y.: Removal of NO and fly ash over a carbon supported catalyst: effects of fly ash concentration and operating time. *Powder Technol.* **239**, 239–247 (2013)
11. Bai, S., Li, H., Wang, L., Guan, Y., Jiang, S.: The properties and mechanism of CuO modified carbon nanotube for NO_x removal. *Catal. Lett.* **144**, 216–221 (2013)
12. Xue, Y., Guo, Y., Zhang, Z., Guo, Y., Wang, Y., Lu, G.: The role of surface properties of activated carbon in the catalytic reduction of NO by carbon. *Appl. Surf. Sci.* **255**, 2591–2595 (2008)
13. Illan Gomez, M.J., Linares-Solano, A., Salinas-Martinez de Lecea, C.: NO reduction by activated carbon. 6. Catalysis by transition metals. *Energy Fuels* **9**, 976–983 (1995)
14. Rosas, J.M.: NO reduction on carbon-supported chromium catalysts. *Energy Fuels* **24**, 3321–3328 (2010)
15. Zhang, G., Li, Z., Zheng, H., Fu, T., Ju, Y., Wang, Y.: Influence of the surface oxygenated groups of activated carbon on preparation of a nano Cu/AC catalyst and heterogeneous catalysis in the oxidative carbonylation of methanol. *Appl. Catal. B* **179**, 95–105 (2015)
16. Rodrigues, E.G., Pereira, M.F.R., Chen, X., Delgado, J.J., Órfão, J.J.M.: Influence of activated carbon surface chemistry on the activity of Au/AC catalysts in glycerol oxidation. *J. Catal.* **281**, 119–127 (2011)
17. Subbaramaiah, V., Srivastava, V.C., Mall, I.D.: Catalytic oxidation of nitrobenzene by copper loaded activated carbon. *Sep. Purif. Technol.* **125**, 284–290 (2014)
18. Ahmad, N., Ibrahim, N., Ali, U.F.M., Yusuf, S.Y., Ridwan, F.M.: Carbon-supported CuO catalyst prepared from oil palm empty fruit bunch (EFB) for low-temperature NO removal. *Proc. Eng.* **148**, 823–829 (2016)
19. Ahmad, N., Yong, S.H., Ibrahim, N., Ali, Md, Fahmi, U.F., Ahmad, M.R.F.R.: Optimisation of Copper Oxide Impregnation on Carbonised Oil Palm Empty Fruit Bunch for Nitric Oxide Removal using Response Surface Methodology. *E3S Web Conf.* 02029, (2018)
20. Rosas, J.M.M., Ruiz-Rosas, R., Rodríguez-Mirasol, J., Cordero, T., Ruiz-Rosas, R., Rodríguez-Mirasol, J., Cordero, T.: Kinetic study of NO reduction on carbon-supported chromium catalysts. *Catal. Today* **187**, 201–211 (2012)
21. Satokawa, S., Shibata, J., Shimizu, K., Satsuma, A., Hattori, T.: Promotion effect of H₂ on the low temperature activity of the selective reduction of NO by light hydrocarbons over Ag/Al₂O₃. *Appl. Catal. B* **42**, 179–186 (2003)
22. Oliveira, L.C.A., Silva, C.N., Yoshida, M.I., Lago, R.M.: The effect of H₂ treatment on the activity of activated carbon for the oxidation of organic contaminants in water and the H₂O₂ decomposition. *Carbon N. Y.* **42**, 2279–2284 (2004)
23. Resitoglu, I.A., Keskin, A.: Hydrogen applications in selective catalytic reduction of NO_x emissions from diesel engines. *Int. J. Hydrog. Energy.* **42**, 23389–23394 (2017)
24. Wang, Y., Zuo, S., Yang, J., Yoon, S.H.: Evolution of phosphorus containing groups on activated carbons during heat treatment. *Langmuir* **33**, 3112–3122 (2017)
25. Prahastha, D., Kartika, Y., Indraswati, N., Ismadji, S.: Activated carbon from jackfruit peel waste by H₃PO₄ chemical activation: pore structure and surface chemistry characterization. *Chem. Eng. J.* **140**, 32–42 (2008)
26. Kalousek, J.: Modelling of NO adsorption in fixed bed on activated carbon. *Chem. Process. Eng.* **32**, 367–377 (2011)
27. Wang, X., Li, D., Li, W., Peng, J., Xia, H., Zhang, L., Guo, S., Chen, G.: Optimization of mesoporous activated carbon from coconut shells by chemical activation with phosphoric acid. *BioResources* **8**, 6184–6195 (2013)
28. Thommes, M., Kaneko, K., Neimark, A.V., Olivier, J.P., Rodriguez-Reinoso, F., Rouquerol, J., Sing, K.S.W.: Physisorption of gases, with special reference to the evaluation of surface area and pore size distribution (IUPAC Technical Report). *Pure Appl. Chem.* **87**, 1051–1069 (2015)
29. Sing, K.S.W., Williams, R.T.: Review physisorption hysteresis loops and the characterization of nanoporous materials. *Ads. Sci. Tech.* **22**, 773–782 (2004)
30. Nowicki, P., Pietrzak, R., Wachowska, H.: Sorption properties of active carbons obtained from walnut shells by chemical and physical activation. *Catal. Today* **150**, 107–114 (2010)
31. Zhong, Z.Y., Yang, Q., Li, X.M., Luo, K., Liu, Y., Zeng, G.M.: Preparation of peanut hull-based activated carbon by microwave-induced phosphoric acid activation and its application in Remazol Brilliant Blue R adsorption. *Ind. Crops Prod.* **37**, 178–185 (2012)
32. Rathore, R.S., Srivastava, D.K., Agarwal, A.K., Verma, N.: Development of surface functionalized activated carbon fiber for control of NO and particulate matter. *J. Hazard. Mater.* **173**, 211–222 (2010)
33. Manyasree, D., Peddi, K.M., Ravikumar, R.: CuO nanoparticles: synthesis, characterization and their bactericidal efficacy. *Int. J. Appl. Pharm.* **9**, 71–74 (2017)
34. Tunesi, M.M., Kalwar, N., Abbas, M.W., Karakus, S., Soomro, R.A., Kilislioglu, A., Abro, M.I., Hallam, K.R.: Functionalised CuO nanostructures for the detection of organophosphorus pesticides: a non-enzymatic inhibition approach coupled with nanoscale electrode engineering to improve electrode sensitivity. *Sens. Actuators B* **260**, 480–489 (2018)
35. Wang, L., Zhou, Y., Liu, Q., Guo, Y., Lu, G.: Effect of surface properties of activated carbon on CO oxidation over supported Wacker-type catalysts. *Catal. Today* **153**, 184–188 (2010)
36. Wang, L., Feng, Y., Zhang, Y., Lou, Y., Lu, G., Guo, Y.: Effect of original activated carbon support and the presence of NO_x on CO oxidation over supported Wacker-type catalysts. *Fuel* **96**, 440–445 (2012)
37. Tang, Y.B., Liu, Q., Chen, F.: Preparation and characterization of activated carbon from waste ramulus mori. *Chem. Eng. J.* **203**, 19–24 (2012)
38. Liu, G., Han, D., Cheng, J., Feng, Y., Quan, W., Yang, L., Saito, K.: Performance of C₂H₄ reductant in activated-carbon-supported MnO_x-based SCR catalyst at low temperatures. *Energies* **12**, (2019)
39. Mangun, C.L., Benak, K.R., Economy, J., Foster, K.L.: Surface chemistry, pore sizes and adsorption properties of activated carbon fibers and precursors treated with ammonia. *Carbon* **39**, 1809–1820 (2001)
40. Bai, B.C., Lee, C.W., Lee, Y.S., Im, J.S.: Modification of textural properties of CuO-supported activated carbon fibers for SO₂ adsorption based on electrical investigation. *Mater. Chem. Phys.* **200**, 361–367 (2017)
41. Goldstein, E.A., Mitchell, R.E.: Chemical kinetics of copper oxide reduction with carbon monoxide. *Proc. Combust. Inst.* **33**, 2803–2810: (2011). <https://doi.org/10.1016/j.proci.2010.06.080>
42. Anuar, A., Yakub, I., Sutan, N.M., Hipolito, C.N.: Temperature-programmed reduction of copper-manganese catalysts derived from biomass activated carbon. *J. Appl. Sci. Process. Eng.* **1**, 28–38 (2014)
43. Kim, J.Y., Rodriguez, J.A., Hanson, J.C., Frenkel, A.I., Lee, P.L.: Reduction of CuO and Cu₂O with H₂: H embedding and kinetic

- effects in the formation of suboxides. *J. Am. Chem. Soc.* **125**, 10684–10692
44. Dandekar, A., Baker, R.T.K., Vannice, M.A.: Carbon-supported copper catalysts. *J. Catal.* **183**, 131–154 (1999)
 45. Streckova, M., Orinakova, R., Hovancova, J., Kobera, L., Brus, J., Hungria, A.B., Girman, V., Mudra, E., Heckova, M., Podobova, M., Kovalcikova, A., Dusza, J.: Fibrous electrocatalytic materials based on carbon/copper/copper phosphides for effective hydrogen evolution. *Appl. Surf. Sci.* **479**, 70–76 (2019)
 46. Subbaramaiah, V., Srivastava, V.C., Mall, I.D.: Catalytic activity of Cu / SBA-15 for peroxidation of pyridine bearing wastewater at atmospheric condition. *AIChE J.* **59**, 2577–2586 (2013)
 47. Hartmann, M., Racouchot, S., Bischof, C.: Characterization of copper and zinc containing MCM-41 and MCM-48 mesoporous molecular sieves by temperature programmed reduction and carbon monoxide adsorption. *Microporous Mesoporous Mater.* **27**, 309–320 (1999)
 48. Velu, S., Wang, L., Okazaki, M., Suzuki, K., Tomura, S.: Characterization of MCM – 41 mesoporous molecular sieves containing copper and zinc and their catalytic performance in the selective oxidation of alcohols to aldehydes. *Microporous Mesoporous Mater.* **54**, 113–126 (2002)
 49. Bard, A.J., Faulkner, L.R.: *Adsorbents: Fundamentals and Applications*. Wiley, Hoboken (2015)
 50. Li, Y., Guo, Y., Zhu, T., Ding, S.: Adsorption and desorption of SO₂, NO and chlorobenzene on activated carbon. *J. Env. Sci. (China)* **43**, 128–135 (2016)
 51. Nabgan, W., Abdullah, T., Mat, T.A., Nabgan, R., Triwahyono, B., Ripin, S.: A.: Hydrogen production from catalytic steam reforming of phenol with bimetallic nickel-cobalt catalyst on various supports. *App. Catal. A* **527**, 161–170 (2016)
 52. Watanabe, M., Aizawa, Y., Iida, T., Nishimura, R., Inomata, H.: Catalytic glucose and fructose conversions with TiO₂ and ZrO₂ in water at 473 K: Relationship between reactivity and acid-base property determined by TPD measurement. *App. Catal. A* **295**, 150–156 (2005)
 53. Shafeeyan, M.S., Daud, W.M.A.W., Houshmand, A., Shamiri, A.: A review on surface modification of activated carbon for carbon dioxide adsorption. *J. Anal. Appl. Pyrol.* **89**, 143–151 (2010)
 54. Shu, Y., Zhang, F., Wang, F., Wang, H.: Catalytic reduction of NO_x by biomass-derived activated carbon supported metals. *Chin. J. Chem. Eng.* **26**, 2077–2083 (2018)
 55. Nikolov, P., Khristova, M., Mehandjiev, D.: Low-temperature NO removal over copper-containing activated carbon. *Colloids Surf. A* **295**, 239–245 (2007)
 56. Xue, Y., Lu, G., Guo, Y., Guo, Y., Wang, Y., Zhang, Z.: Effect of pretreatment method of activated carbon on the catalytic reduction of NO by carbon over CuO. *Appl. Catal. B* **79**, 262–269 (2008)
 57. Zhu, Z.H., Radovic, L.R., Lu, G.Q.: Zhu, Radovic, Lu - Effects of acid treatments of carbon on N₂O and NO reduction by carbon-supported copper catalysts—Carbon.pdf. *Carbon* **38**, 451–464 (2000)
 58. Li, Q., Yang, H., Ma, Z., Zhang, X.: Selective catalytic reduction of NO with NH₃ over CuOX-carbonaceous materials. *Catal. Commun.* **17**, 8–12 (2012). <https://doi.org/10.1016/j.catcom.2011.10.008>
 59. Chattopadhyaya, G., Macdonald, D.G., Bakhshi, N.N., Mohammadzadeh, J.S.S., Dalai, A.K.: Removal of nitric oxide over Saskatchewan lignite and its derivatives. *Catal. Lett.* (2006). <https://doi.org/10.1007/s10562-006-0029-7>
 60. Plaza, M.G., Pevida, C., Arias, B., Feroso, J., Arenillas, A., Rubiera, F., Pis, J.J.: Application of thermogravimetric analysis to the evaluation of aminated solid sorbents for CO₂ capture. *J. Thermal Anal. Calorim.* **92**, 601–606 (2008)
 61. Papirer, E., Li, S., Donnet, J.B.: Contribution to the study of basic surface groups on carbons. *Carbon* **25**, 243–247 (1987)
 62. Dandekar, A., Baker, R.T.K., Vannice, M.A.: Characterization of activated carbon, graphitized carbon fibers and synthetic diamond powder using TPD and DRIFTS. *Carbon* **36**, 1821–1831 (1998)
 63. Chen, L., Ma, D., Bao, X.: Hydrogen treatment-induced surface reconstruction: formation of superoxide species on activated carbon over ag/activated carbon catalysts for selective oxidation of CO in H₂-rich gases. *J. Phys. Chem. C* **2**, 2229–2234 (2007)
 64. Hsu, L.Y., Teng, H.: Influence of thermal treatment on the catalytic activity of Cu-loaded carbons in NO reduction with NH₃ and regeneration of the thermally deactivated catalysts. *Appl. Catal. B* **42**, 69–76 (2003)
 65. Dong, F., Meng, Y., Han, W., Zhao, H., Tang, Z.: Morphology effects on surface chemical properties and lattice defects of Cu/CeO₂ catalysts applied for low-temperature CO oxidation. *Sci. Rep.* **9**, 1–14 (2019)

Publisher's Note Springer Nature remains neutral with regard to jurisdictional claims in published maps and institutional affiliations

Affiliations

N. Ahmad¹ · F. M. Zahari¹ · N. Ibrahim¹ 

¹ School of Environmental Engineering, Universiti Malaysia Perlis, Kompleks Pusat Pengajian Jejawi 3, 02600 Arau, Perlis, Malaysia